

MICROSTRUCTURE SIMULATIONS

A. AKSI^(a), A. CHOUDHURY^(a), S. SCHULZ^(a), C. MENNERICH^(a), A. MELCHER^(a), B. NESTLER^(a)

^(a) Institute of Materials and Processes
Karlsruhe University of Applied Sciences
Moltkestr. 30, 76133 Karlsruhe, Germany
Phone: +49 (0)721 925 1504,
Fax: +49 (0)721 925 1503
britta.nestler@hs-karlsruhe.de

ABSTRACT

For developing new materials and optimizing processes, the simulation of microstructure formations and the computational investigation of influences from process conditions, alloy composition and external fields have gained essential importance for academic research as well as industrial applications. The phase-field method has demonstrated a wide potential in various applications to describe complex phase transitions and pattern formations. We apply a phase-field model for multicomponent and multiphase systems to microstructure formations in materials such as biological, geological systems and metallic alloys. We introduce extensions for inert particles obeying volume constraints and for coupling with fluid flow. To solve the dynamical equations, an extensive software package *pace3D* with parallel and adaptive algorithms has been developed. The influence of various physical quantities on the microstructure properties can be evaluated by systematic parameter studies. We present microstructure simulations for different material systems, process conditions and external forces.

1. INTRODUCTION

During the manufacturing process of almost all kinds of materials, the characteristic quantities of the evolving microstructures strongly determine the mechanical properties of the resulting components. Depending on the process conditions and the material data, different phase transitions occur leading to various types of growth morphologies. The microstructure formation process has a great influence on the quality of the material and on the durability of the component. Modern computational methods provide a great potential to tailor material with specific properties and to virtually design production processes.

pace3D is a massive software package for large 3D parallel simulations, data analysis and high quality visualization of microstructure formation processes in metallic alloys and other materials such as ceramics, geological or biological systems. The simulator includes methods to compute various effects such as phase transformation processes in multi-component multiphase systems under the consideration of mass and heat diffusion, convection, anisotropy and elasticity. Another aim is to numerically study multi-scale phenomena occurring on different time and length scales. Separate program modules to solve the phase-field equations, the Navier-Stokes equations, the Lattice Boltzmann model for fluid flow or the evolution of elastic stresses can be loaded. The package contains:

- Pre-processing tools for data preparation: Configuration of material parameters, initialization of the computational domain and conversion of experimental data sets
- Main-processing: Simulation techniques for numerically solving the set of evolution equations including parallel and adaptive grid methods as well as memory and computation time optimizations
- Post-processing tools: Data analysis and high quality visualization

The implementation is done in C, C++ under a Linux environment. Simulations can be performed sequentially or parallel on high performance clusters using MPI. The algorithms contain adaptive staggered grids and SSOR-methods.

In this overview article, we introduce simulation results of microstructure evolutions in biological, geological and metallic material systems. In Section 2, we show the motion of cells in veins including the interaction of the cells with the wall and the interaction between cells. In Section 3, we describe the use of

thermodynamical data bases in order to compute microstructures on the basis of real material data. In Section 4, we demonstrate the applicability of the methodology to investigate crack-sealing processes in geological rocks. The presentation is finalized by a discussion on the transfer of experimentally measured data of polycrystalline grain structures to initialize the computational domain.

2. SIMULATION OF BLOOD CELLS IN VEIN SYSTEMS

Erythrocytes, also known as red blood cells; are one of the most important components in the human bloodstream. They supply the body tissue with oxygen via the blood. An important parameter in conventional blood tests is determining the number of red blood cells per volume.

In order to investigate issues, such as agglomeration of blood cells in vein systems and bifurcations as it occurs during atherosclerosis, an analytical model is needed to analyze blood flow and dynamics. For our simulations we use a formulation of a phase-field model which incorporates order parameters with preserved volume representing cells and particles evolving in a system such that the interfacial energy decreases. As a first approach we approximate the red blood cells as round particles. The particles are defined as regions with energy bearing boundaries that may differ in their physical states. A Lattice-Boltzmann method is used to describe the motion of the particles in a flow field.

2.1. Simulation of vein Systems

In order to simulate a vein system, we use a voronoi algorithm in 3D which generates a random distribution of different phases. At triple points of these phases, we then set round liquid phases which form a 3D channel structure. Fig. 1 and 2 show a possible configuration of a vein system which can be used to study the flow dynamics of blood cells.

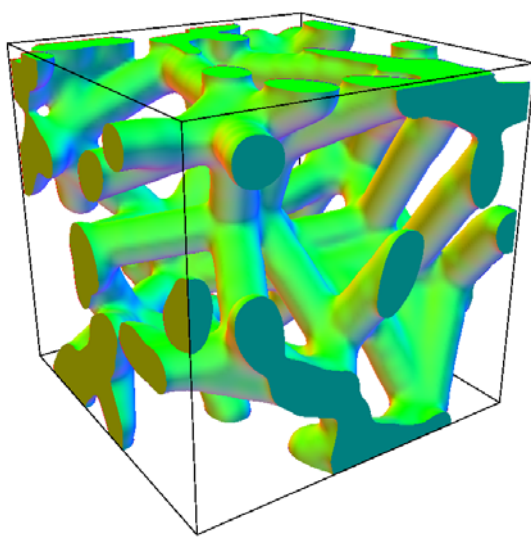


Figure 1: A possible structure of a vein system

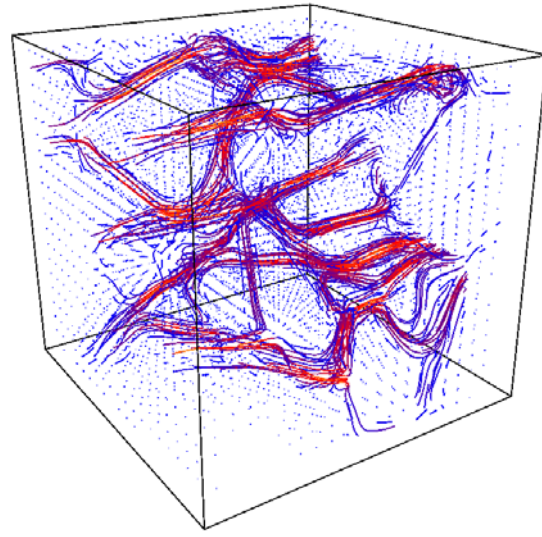


Figure 2: Streamlines of the fluid flow through the vein system

2.2. Simulations for studying the behavior at bifurcations

The results from our simulations match closely the observations made in experimental investigations of blood flow at bifurcations. Fig. 3 and 4 show the simulation results with two droplets. Fig. 5 shows the corresponding experimental observation.

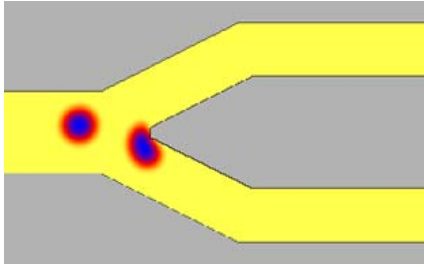


Figure 3: Striking of cells at the bifurcation

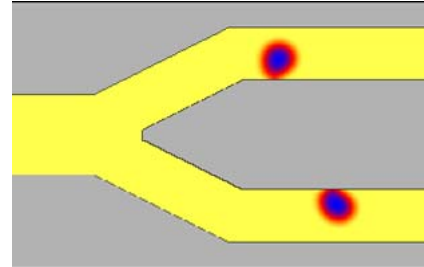


Figure 4: Interaction of cells with the wall

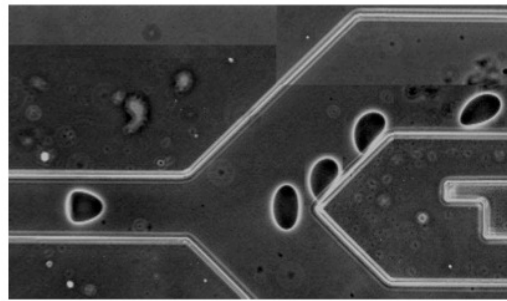


Figure 5: Experimental results (Gwennou Coupier)

2.3. Computational study of effective viscosity

Blood is from the physical point of view a suspension. It is a mixture of a liquid or water component and cellular components. It is a non-Newtonian fluid, which is the reason for its specific flow characteristics. Because of the contained erythrocytes, blood has a larger viscosity range than plasma. By increasing the hematocrit value and decreasing the velocity of the flow, the effective viscosity of blood will increase. Because of the deformability of the blood cells at high velocities, blood does not longer behave like a suspension but rather like an emulsion.

At low levels of erythrocyte volume fractions and at a certain velocity of the flow, the blood cells arrange themselves in a row shape in the middle of the capillary to minimize the flow resistance. The arrangement in the middle of the capillary is like the zip merging procedure. Fig. 6 shows a snapshot of one of our simulations. The arrangement of droplets in a shear flow can be seen. The zip merging of the cells can also be seen. This behavior of red blood cells is well known. It was first observed in 1969.

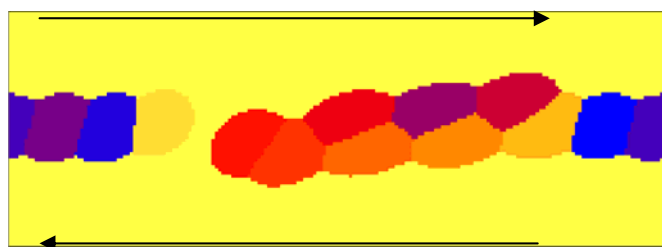


Figure 6: Arrangement of droplets in a shear flow in the middle of the capillary

One of the most important properties of blood is that it is a non-Newtonian fluid and thus exhibits special characteristics in its flow properties. One of these properties is the behavior of the effective viscosity by a certain volume fraction of red blood cells at different diameters of the blood vessel.

For investigating the effective viscosity of a dilute suspension we did 2D simulations for different types of domains with different amounts of particles, distributions and volume fractions. We have approximated the suspension as a liquid phase containing spherical particles which are also defined as liquid phases with a higher viscosity than the solvent. For evaluating the effective viscosity of the suspension, we apply a shear flow and calculate the effective viscosity by choosing a constant radius of the particles and a constant shear rate and by varying the volume fraction of the particles and the wall-to-wall distance of the simulation

domain. The boundary condition at the closed walls (bottom and top) is no-slip. At the particle-fluid phase boundaries, a diffuse no-slip boundary condition is modeled. The particles stick together because of their surface tension and they rotate in the shear flow.

By evaluating simulation results, we found an interesting characteristic of the effective viscosity, which looks very similar to the Fahraeus-Lindqvist effect which is well known for blood flowing through capillaries of different diameters. Blood flow in small blood vessels needs a special consideration. The absolute size of the particles in comparison to the whole domain cannot be neglected any more.

The changing viscosity of blood as a function of blood vessel diameter and volume fraction of red blood cells is called “Fahraeus Lindqvist Effect”. The effective viscosity decreases with decreasing blood vessel diameter. This is caused by increased interactions between the blood cells and the separation of hematocrit and plasma. So the blood cells move over the center of the vessel to minimize the flow resistance. And this is the effect that we also discovered in the simulations. Fig. 7 indicates the effective viscosity for different volume fractions of particles as a function of the dimensionless gap. (Wall-to-wall distance $C = w/2R$).

At concentrations higher than 15%, the effective viscosity decreases, when the inter-wall distance gets closer and decreases. For smaller concentrations, the effective viscosity is nearly constant.

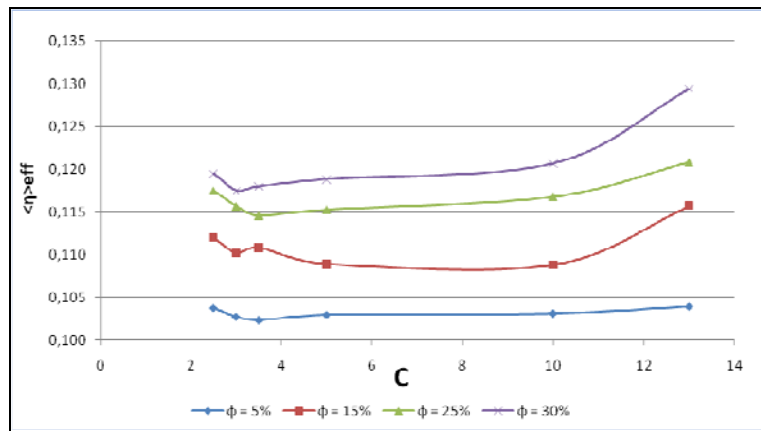


Figure 7: The effective viscosity for different volume fractions as a function of the dimensionless gap

Fig. 8 shows the evaluated effective viscosity as a function of the volume fraction for different wall-to-wall distances C .

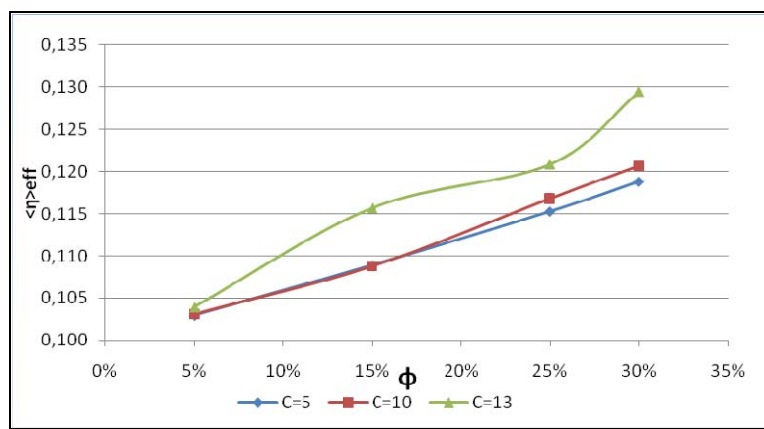


Figure 8: The effective viscosity as a function of the volume fraction

2.4. Future Work

It is planned to conduct simulations in 3D and run further simulations with different ratios of particle viscosity and solvent viscosity. Furthermore we will consider more properties of the blood cell membrane in our model and investigate the impact of these properties. Modeling the complex shape of red blood cells will

also be a part of the future work because the shape of the red blood cells has a great influence to the flow behavior.

3. UTILISATION OF THERMODYNAMIC DATABASES FOR PHASE-FIELD MODELING

To derive results out of phasefield simulations which are representative of a real alloy, precise thermodynamic properties of the system to be investigated are required as input values. For simulations with the *pace3D* software up to now, ideal, regular and sub-regular free energy models were used to describe the thermodynamic properties (free energies) of the different phases. The required parameters for the free energies are taken as input and are set manually in the infile for the solver. An alternative would be the automatic access of thermodynamic datasets, which are used for calculation of phase diagrams using the Calphad-method (www.calphad.org), for utilization in the solver. In this report we present a coupling of thermodynamic datasets to the *pace3D* simulation software and thereby achieve results from simulations of the aluminium-copper system.

3.1. Utilization of thermodynamic databases for phasefield- simulations

In general, thermodynamic datasets are used for the calculation of phase diagrams according to the Calphad-method which is implemented in several commercial software-products such as ThermoCalc (Thermo-Calc Database Guide, 2006) or Pandat (Pandat 7 Users Guide, 2007). On the basis of a variety of experimental data, such datasets are available for most of the commercially important alloys and have been verified extensively. They contain a description of the Gibbs free energy of different phases, from which other thermodynamical values can be obtained, such as the chemical potential or the heat capacity. There exist several models with which the Gibbs free energy can be described through mathematical expressions, or formalisms. Most of the formalisms are special cases of the *Compound Energy Formalism* (Hillert, 2001) which considers phases with an arbitrary amount of sublattices and components.

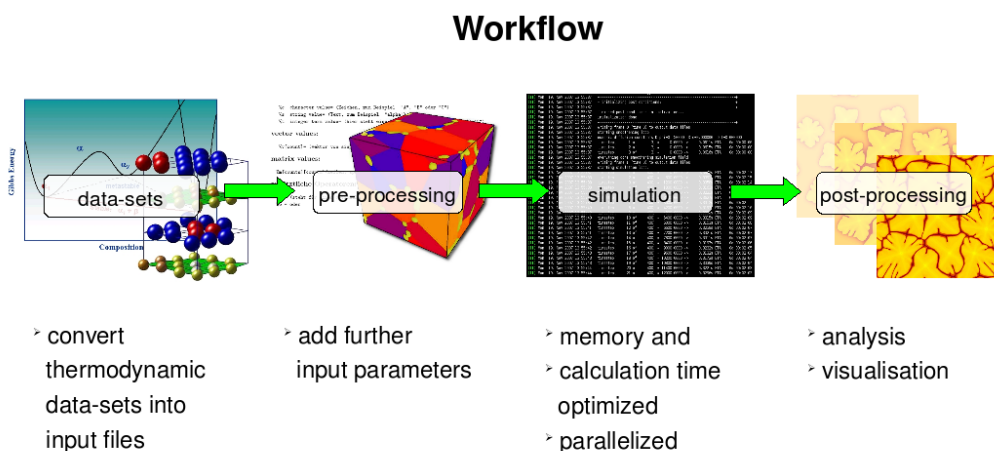


Figure 9. Workflow for phasefield simulations with *pace3D*, using thermodynamic datasets.

These datasets can also be used for phasefield-simulations, as shown in Fig. 9. By a converting-program, the thermodynamic data can be written into an input-file, in which further simulation-parameters have to be appended manually. The solver of *pace3D* has now an additional implementation of the *Compound Energy Formalism*, by which the thermodynamic input-data can be used for the calculation of the simulation. The results obtained after the simulation can be visualized and validated.

3.2. Simulation results

By utilizing the thermodynamic dataset of aluminium-copper a simulation of this system has been carried out. The simulation was done within a two-dimensional calculation domain at a constant undercooled temperature of 830K and a copper-concentration of 0.09 in the melt. In this case the system is located in the two-phase region between the liquidus and the solidus line, in which both the liquid and the solid phase exist. In the initial state the domain is filled with an undercooled melt with a copper-concentration of 0.09. In the middle of the domain two circular nuclei of the aluminium-rich alpha-phase have been set. Their copper-

concentration has been chosen to 0.022, that corresponds to the equilibrium concentration of this phase at the given temperature.

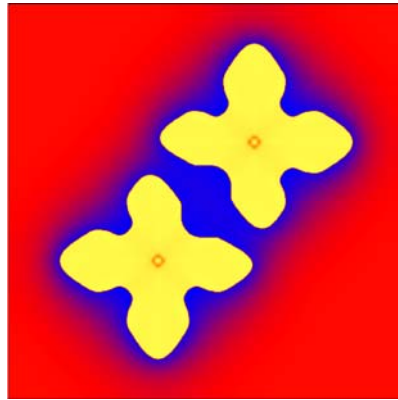


Figure 10. Final state of the simulation of the solidification in an aluminium-copper alloy. Aluminium-poor melt is located between the dendrites.

At the final state (Fig. 10), the nuclei have evolved into two dendrites with four main-arms. Between the dendrites (depicted as yellow), a region of aluminium-poor melt (depicted as blue) has developed, the copper-concentration of 0.17 matches to the equilibrium concentration of the liquid phase at this temperature.

3.3. Outlook

To achieve the intended objective of using thermodynamic datasets for phasefield simulations in its whole extent, several possibilities arise for the future. In the long term the converting program could also be integrated into the *pace3D-Studio*, which is an infile-editor with a graphical user-interface. The newly implemented solver function for the *Compound Energy Formalism* should be validated through simulations of different material systems. The investigation of the aluminium-copper system could be continued by a simulation of interdendritic, eutectic growth, as shown in Fig. 11, where one can see the result of a simulation done with the ideal free energies for the phases.

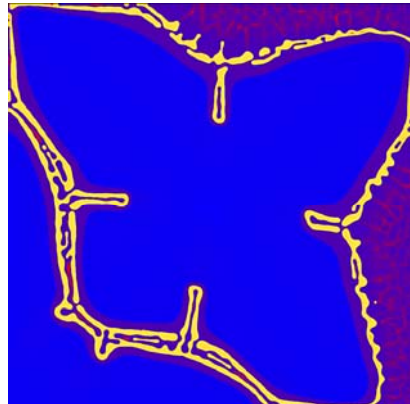


Figure 11. Interdendritic, eutectic growth, simulated with the previous method.

By the addition of further models for the Gibbs free energy to the solver, datasets including ions, vacancies or effects like magnetism could also be used for phasefield simulations. Finally, new datasets for ternary or higher component alloys could be investigated or available binary sets could be combined to create datasets for microstructure simulations.

4. GRAIN STRUCTURE FORMATION IN GEOLOGICAL MATERIALS

Zeolites (Greek: *zeon*: boiling, *lithos*: stone) as special crystals are of great interest (cp. Caro *et al.*, 1999). They occur naturally and may therefore be involved in the process of sealing stone wall cracks in groundwater or oil reservoirs, but are also grown artificially on thin films for industrial purposes, where special preferred orientations are wanted to obtain dedicated physical properties. In the following, simulation results for polycrystalline competitive grain growth in zeolite-like structures on the one hand, and in the mechanisms in sealing cracks as observable in rock veins on the other hand, are given. For these simulations of grain growth of geological materials, a phase-field model, originally developed for metallic systems on a mesoscopic scale, was adapted and extended. The shown simulation results are generated by the software package *pace3D* (developed and maintained at the Institute of Materials and Processes (IMP) at the University of Applied Sciences, Karlsruhe), which includes a solver for the evolution equations of the phase-field model as well as a variety of pre- and post processing tools to analyze and visualize the results.

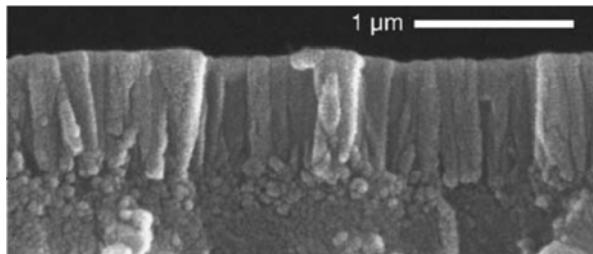


Figure 12: Zeolites growing on a thin film (the picture is taken from Bons and Bons (2003)).

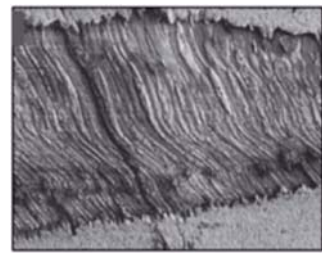


Figure 13: A vein in a host rock.

4.1. Orientation distribution and modeling of faceted anisotropy

On the formation of characteristic geometries and properties in grain growth, the orientation of the initial grains has a great influence. Therefore, a good initial distribution of orientations is needed. For two-dimensional problems this can be done by marking equidistant points on the unit circle of a global coordinate system and using these points as orientations, where existing symmetries of the grains have to be taken into account appropriately (see Fig. 14).

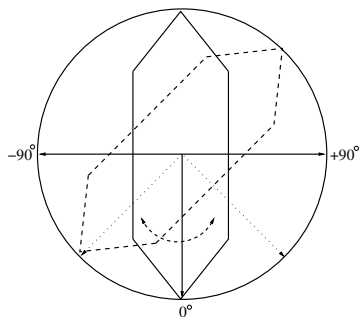


Figure 14: A six-cornered symmetric shape in the unit circle.

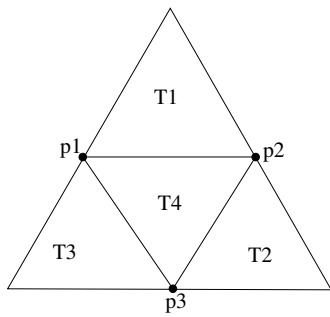


Figure 15: Tessellation of triangle.

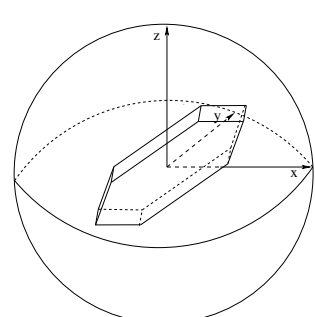


Figure 16: A coffin shaped figure in the unit sphere.

Angle distribution in three dimensions is more complicated. The division of the unit sphere in three-space into equidistant circles (as known from terrestrial globes) results in circles of different diameters and leads to formation of poles, and therefore to a non-uniform angle distribution. As an approximation to a uniform point distribution the following approach is used: An icosahedron (a Platonic solid with 20 triangular facets) is inscribed into the unit sphere. The facets of the icosahedron are tiled into four new ones by connecting the midpoints of their sides (in analogy to the Sierpinski tessellation in fractal geometry, cp. Fig. 15) and projecting these midpoints back onto the unit sphere. This procedure is repeated, so that after n iterations

(with F_i and P_i the numbers of facets and points in iteration i respectively, and the index 0 indicating the original icosahedron) holds

$$F_n = 4 \cdot F_{n-1} \quad (1)$$

$$P_n = \frac{3}{2} \cdot F_{n-1} + P_{n-1} \quad (2)$$

or, written as closed expressions

$$F_n = 20 \cdot 4^n \quad (3)$$

$$F_n = 10 \cdot 4^n + 2 \quad (4)$$

For the formulas derivations only the properties of convex polytopes are used (for further information see Grünbaum, 1967). Results of successive tiling steps can be seen in Table 1 and Fig. 17.

Table 1: The numbers of points and facets after different tiling steps.

Iteration	Number of points	Number of facets
0	12	20
1	42	40
2	162	320
3	642	1280
4	2562	5120

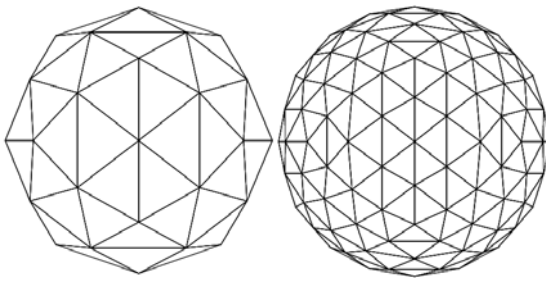


Figure 17: An icosahedron after two and three tiling steps.

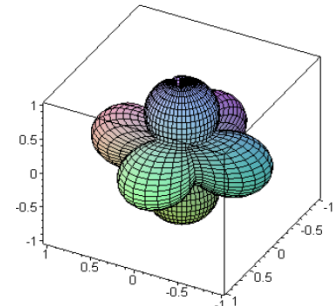


Figure 18: Wulff-plot of a six-cornered octahedral shape.

The obtained points serve as growth direction for grains in simulations by rotating a grain in such a way that its local x-axis shows in direction of this point. To create arbitrary crystal shapes, an anisotropy function is needed. The energy of a crystal can be described in terms of its orientation dependent surface energy, displayed in the so called Wulff-plot. Its equilibrium shape is then given as the inner envelope of the normals to the graph of this anisotropy function (see Gottstein, 2003). For the simulations shown here the function

$$\max\{\mu_k \cdot n / k = 1, \dots, N\} \quad (5)$$

is used (where the vectors μ_k are vectors to the corners of an N-cornered shape, n is the normal to the crystals facets and \cdot denotes the standard scalar product in Euclidean three-space). This function produces a sharp faceted anisotropy. Fig. 18 shows the Wulff-plot for a six-cornered octahedral shape.

4.2 Zeolite-like grain structure growth

Referring to Bons and Bons (2003) zeolite shapes can be approximated by coffin-like shapes with differing aspect ratios and a certain thickness (cp. Fig. 16). During the growth of zeolites on thin films, oblique crystallographic orientations occurred, but were overgrown by grains with straight orientations (i.e. grains with an orientation with small angular deviation from the substrate normal) in later stages of the film growth. This grain behavior has been simulated in two and three dimensional settings. The final geometry of a 2D simulation with 180 initially equidistant grains of equal size with orientations differing from tois is shown in Fig. 20. In this simulation it can be observed how grains with oblique orientations are overgrown by grains with straight orientations (colored in red) after a sufficiently long time of competitive grain growth (see the chart in Fig. 19 and Fig. 20 and 21).

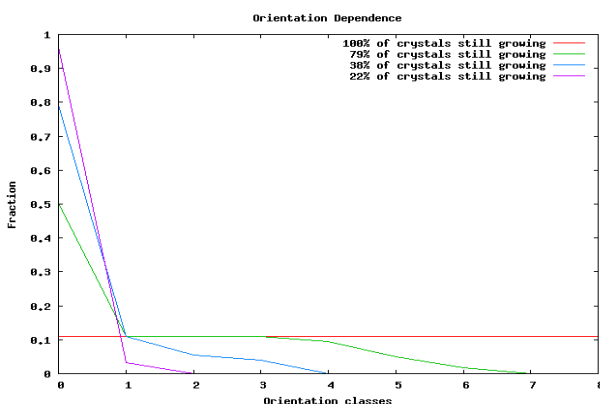


Figure 19: The fraction of different orientations is plotted (orientations are grouped in classes of deviation from the substrate normal) for different amounts of still growing grains.

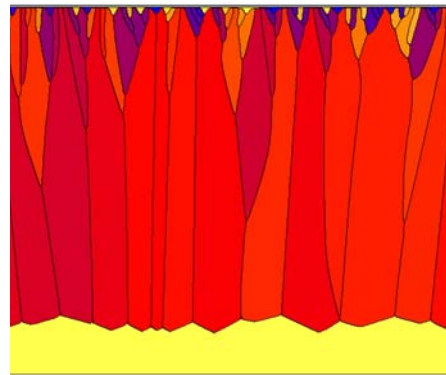


Figure 20: 2D simulation of competitive grain growth with outgrowing oblique orientations.

Similar settings have been analyzed in 3D. A system of 25 zeolite-shaped grains with aspect ratio 4:1 can be seen in Fig. 22. In 3D, similar competition mechanisms are valid as well as in two dimensions, so that oblique orientations are overgrown by straight ones when growth competition starts to take place (see also Fig. 22).



Figure 21: Outgrow of an oblique orientated grain in a 2D competitive grain growth scenario.



Figure 22: Three stages of 3D grain growth of 25 randomly orientated grains. Oblique orientations are overgrown.

4.3 Crack-seal processes

Natural rocks underlay strong tectonics and other geological activities, what might lead to micro-cracks in which hyper-thermal, supersaturated aqueous mineral solutions can seep into. Diffusion and advection allow polycrystalline grain growth by which the crack is sealed (this procedure is called crack-seal process (Ramsey, 1980)). Growth competition between the polycrystals results in characteristic crack-seal lamellae.

On their formation, the initial orientation and size of the grains as well as their neighborhood and the roughness of the host rock wall have a great influence (cp. (Hilgers *et al.*, 1999)). The process of sealing cracks in a host stone matrix has been simulated with focusing on uniaxial grain growth (i.e. growth starting on exactly one side of the crack wall into a liquid phase). In this process, many different additional parameters are involved, such as the roughness of the wall where the growth starts, the roughness of the crack and its shear rate. The survival rate for the orientations correlates with the direction of the shear of the crack, so that grains with oblique orientations occur in late stages of successively applied crack-seal processes if they grow in the direction of the shear. We here assume a complete sealing of cracks, i.e. the growth speed of the crystals is much higher than the occurrence of crack events. If the frequency of the crack events is higher than the growth of the crystals, this results in an open cavity growth (so that growth competition is not affected by the crack events). Fig. 23 shows the results for several crack-seal cycles with a shearing crack. Formation of characteristic lamellae can be observed.

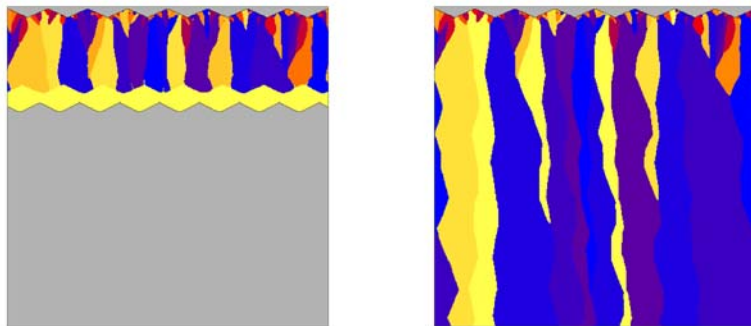


Figure 23: Two time steps of a crack-seal process with a 20 pixel shear to the right. Grains growing in shear direction survive the competition, characteristic lamellae evolve.

4.4 Conclusions

The phase-field model proved to be an appropriate tool to examine polycrystalline competitive grain growth in geological materials as well as on thin films. The faceted anisotropy function used creates sharp shaped geometries and therefore is well-suited to approximate real crystal shapes on small scales. Next steps towards a deeper understanding in the formation processes in geological materials are simulations in large three dimensional settings (361 grains with different orientations but same aspect ratio competing on smooth substrated films).

5. CONVERSION OF EXPERIMENTAL EBSD-DATA TO PHASE-FIELD SIMULATION DATA IN A POLYCRYSTAL

In a polycrystal the several grains can be distinguished in terms of the orientation expressed in Eulerian angles. In order to study the orientation of the grains, Electron Backscatter Diffraction (EBSD) is performed in a scanning electron microscope. The measurement is given in Eulerian angles and from this it is possible to reconstruct the grain structure of the sample via the misorientation between two grains in a quaternion based algorithm. This procedure gives a two-dimensional representation of information in physical three dimensional space.

In this section, we describe the conversion algorithm from experimentally measured data to simulation data in detail. First we introduce the EBSD-measurement. In the second subsection we state the basic mathematical formulas for quaternions. Then we describe the conversion algorithm and present some result. Finally we give a short outlook of the possible extension for the three dimensional case.

5.1 EBSD-Measurement

A stationary electron beam is focused on the 70° tilted sample and the diffracted electrons form a pattern on a fluorescent screen (see Fig. 24). This pattern is characteristic of the crystal structure and orientation of the sample region from which it was generated. The data are evaluated with a special software. The results of the

measurement are available as a text file and as pictures. The main information is the spatial points where the measurement takes place in Eulerian angles.

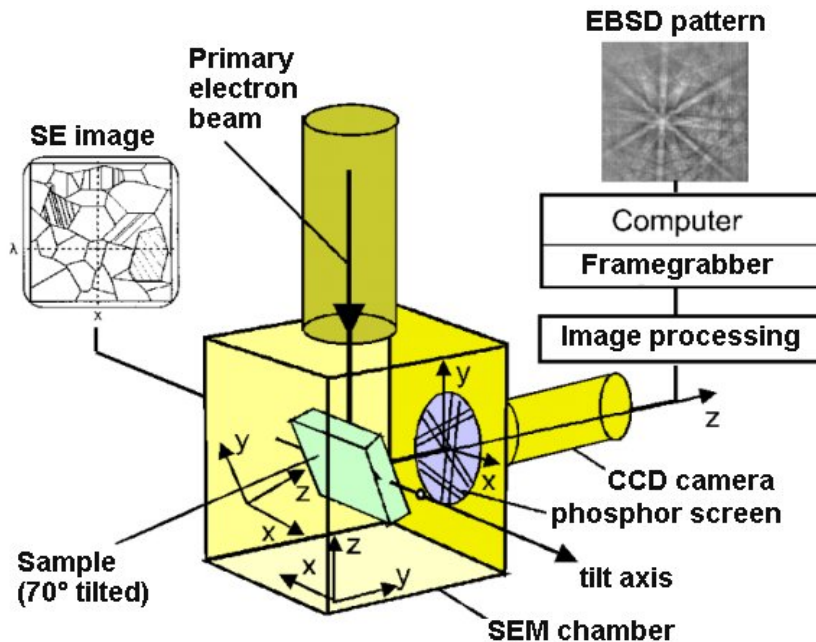


Figure 24: Scheme of EBSD measurement. (Source IFW Dresden)

From the EBSD-data, we are able to reconstruct the following microstructure quantities:

- content of phases, size and shape of grains, misorientation within deformed grains
- grain boundary type (misorientation angle, CSL classification)
- texture results like pole figures, inverse pole figures, ODF, fractions, indices...

In the following application we restrict our concern to the reconstruction of the shape of grains.

5.2 Mathematical Basics of Quaternions

To describe a three-dimensional rotation resp. orientation, it is well known (Morawiec, 1989) that there exists a strong relation between Eulerian angles (α, β, γ), rotation axis \mathbf{n} angle ω and quaternions. The advantage of using quaternions is that the singularity of the origin of the Euler angle space is avoided. In the sequel (Cho, 2005), we introduce the important formulas needed in our conversion algorithm.

A unit quaternion \mathbf{q} is an ordered set of four real numbers:

$$\mathbf{q} = (q_0; \mathbf{q}) \text{ satisfying } \sum_{i=0}^3 q_i^2 = 1. \quad (6)$$

The connection to the Eulerian angles is given through

$$\mathbf{q} = \left(\cos \frac{\theta}{2} \cos \frac{\alpha + \gamma}{2}; -\sin \frac{\theta}{2} \sin \frac{\alpha + \gamma}{2}, \sin \frac{\theta}{2} \cos \frac{\alpha - \gamma}{2}, \cos \frac{\theta}{2} \sin \frac{\alpha - \gamma}{2} \right) \quad (7)$$

The inverse rotation in terms of quaternions is

$$\mathbf{q}^{-1} = (q_0; -\mathbf{q}) \quad (8)$$

and the multiplication of two quaternions $\mathbf{q}^1, \mathbf{q}^2$ is defined as

$$q^1 \cdot q^2 = (q_0^1 q_0^2 - q^1 \cdot q^2; q_0^1 q^2 + q_0^2 q^1 + q^1 \times q^2). \quad (9)$$

Then the misorientation of two grains in terms of quaternions is given as

$$M = (q^1)^{-1} \cdot q^2 \cdot S_i \quad (10)$$

where the S_i is a crystal symmetry dependent quaternion. In a cubic crystal we have to consider 24 quaternions S_i and therefore 24 misorientations have to be computed, where the minimum value is taken as misorientation.

5.3 The Algorithm

With the formula (6)-(10) we are able to describe the core of our conversion algorithm. In a first step all orientations of the measurements points are transformed in a corresponding quaternion via formula (7). According to equations (8) - (10) we compute the misorientation in a measurement point with its neighbors. In the next step we perform a cluster analysis due to a threshold argument, that means if the misorientation is lower than a specified threshold the two orientations from where we have computed the misorientation belongs to the same class. Additional conditions are also necessary to make the cluster analysis unique. In the final step we compute for every identified cluster the normalized arithmetic mean in terms of quaternions as

$$\bar{Q} = N^k \sum_{i=1}^{2N_k} Q_i \text{ with } \|\bar{Q}\| = 1. \quad (11)$$

where N^k is a normalization factor and N_k are the elements of the k-th cluster. Finally we reconstruct from these data the spatial distributions of the grains in the polycrystal. We note that addition to the steps described above, several other steps like filtering and measurement error removal are processed to gain more quality and accuracy in the converted data to get an optimal reconstruction of the grain structure.

5.4 Results and Outlook

In this section, we compare the original data coming from the EBSD measurement with the data we receive from our conversion algorithm. The image in Fig. 25 is generated from original EBSD software. The top image in Fig. 26 shows the result of the conversion algorithm without filtering and error removal, while the lower image in Fig. 26 shows the result with filtering and error removal. It can be seen in Fig. 25 that we are also reconstruct a grain structure in areas where the EBSD-measurement failed. But this is taken with care. In the other areas we have a good agreement between the original EBSD data and the reconstructed data.

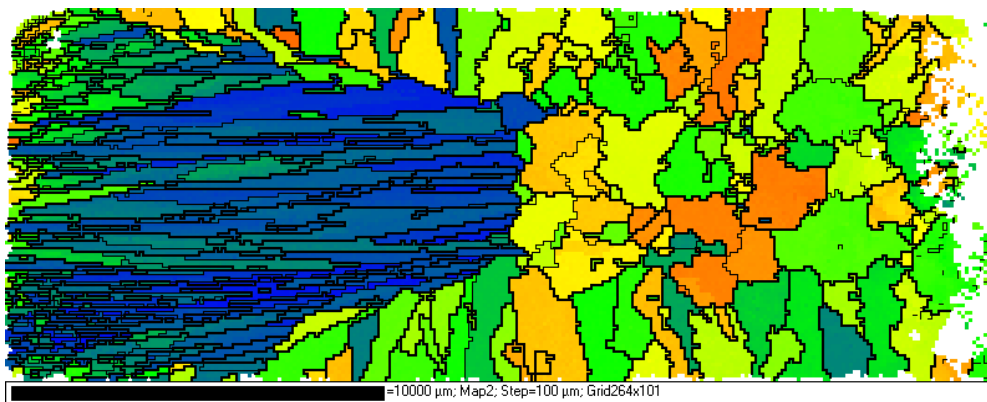


Figure 25: Measurement from EBSD-software (Source: IFW Dresden)

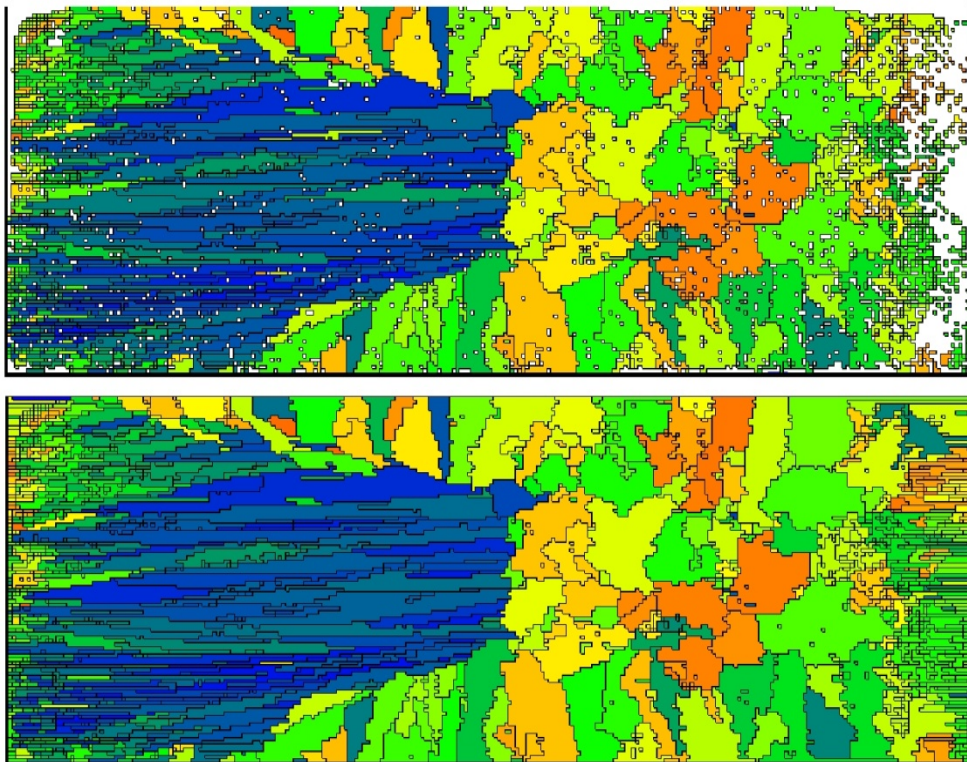


Figure 26: Converted data without and with filtering and error removal (top and bottom image, respectively).

Now the reconstructed data can be used as initial data for the phase-field simulation. The advantage is the very good reconstruction of the grain structure. But additional physical information like surface energy or elastic properties cannot be given by this measurement a priori. And therefore additional research is necessary. Furthermore the reconstruction of 3D structures is also a difficult task. If EBSD measurements of a 3D sample are provided for different layers, we can reconstruct the 3D structure straightforward from the algorithm above, when we extend our ideas in the third space dimension. The experimental method is restricted to materials where the mechanical preparation for the EBSD measurement does not change the microstructure of the sample.

REFERENCES

1. Bons A-J., Bons P.D. 2003, The development of oblique preferred orientations in zeolite films and membranes, *Microporous Mesoporous Mater.* 62: 9-16
2. Caro J., Noack M., Kölsch P., Schäfer R. 1999, Zeolite membranes - state of the their development and perspective, *Microporous Mesoporous Mater.* 38 (2000): 3-24
3. Cho J.H., Rollett A.D., Oh K.H. 2005, Determination of a Mean Orientation in Electron Backscatter Diffraction Measurements. *Metallurgical and Material Transcations A*, Vol. 36A, pp. 3427-3438.
4. Gottstein G. 2007, *Physikalische Grundlagen der Materialkunde*, Springer, Berlin, 502p.
5. Grünbaum B. 1967, *Convex Polytopes*, Interscience Publishers, London, 456p.
6. Hilgers C., Koehn D., Bons P.D., Urai J.L. 1999, Development of crystal morphology during unitaxial growth in a progressively widening vein: II. Numerical simulations of the evolution of antitaxial fibrous veins, *J. Struct. Geol.* 23 (2001): 873-885
7. Hillert, M. 2001, The compound energy formalism, *Journal of Alloys and Compounds*, (2001), Ausgabe 320, Seiten 161-176
8. Morawiec A., Pospiech J. 1989, Some Information on Quaternions Useful in Texture Calculations, *Textures and Microstructures*, Vol. 10, pp. 211-216.
9. Pandat 7 User's Guide, ComuTherm LLC, 2007
10. Ramsey G.J. 1980, The crack-seal mechanism of rock deformation, *Nature* 284: 135-139
11. Thermo-Calc Database Guide, Foundation of Computational Thermodynamics, 2006
12. www.calphad.org